ON THE MAGNUS ROTATING ROLL STABILIZER; NUMERICAL AND EXPERIMENTAL STUDIES

Ö. İlkan Aydın[1], Hakan Akyıldız[2]
1 İstanbul Technical University | aydinozd@itu.edu.tr
2 İstanbul Technical University | akyildiz@itu.edu.tr

ABSTRACT

Magnus rotating roll stabilizer is a roll reduction device that it generates lifting force installed at the bilge of ship's hull as an alternative of anti- rolling system. In this study, hydrodynamic characteristics in terms of a ship's roll-heave motions in a regular beam sea and anti-rolling effects at low/medium speed in the varied rotation speeds are investigated in details. For practical purposes, the calculation model of the anti-rolling force is established with the vertical velocity components caused by ship roll motion into consideration. Magnus lift force produced by the rotating cylinders in the fluid field were calculated by the numerical simulation and towing experiment. The simulation results for two-dimensional rotating cylinders and three-dimensional ship-rotor cases show that Magnus rotating roll stabilizer is more suitable and effective with high performance for ship roll stabilization at low/medium speed.

Keywords: Magnus effect, rotating circular cylinder, roll damping, numerical simulation, towing experiment

1. Introduction

When a ship sails across the sea, six degrees of freedom motions could be generated and the roll motion has a more severe impact than the other five degrees of freedom motions. Large roll motion can lead to increasing the sailing resistance, cargo damage, effect the normal work of shipboard equipment, motion sickness and ship capsizing [1, Perez and Blanke, 2012]. Roll motion at low speed has strong nonlinear features with bigger roll amplitude than that in high speed. Ships experience larger roll motion at lower speed as the roll damping decreases with the decrease of sailing speed. In this circumference, with the development of ship industry, the working conditions of ship mission profile at low/medium and zero speed are more common, such as ship-based helicopters taking off and landing and work boats lowering and hoisting etc. [2, Liang et al., 2015]. Therefore, roll reduction at low/medium speed becomes the future development direction of roll stabilization research field [3, Zhang et al, 2012].

The common roll reduction devices at low speed are anti-rolling tanks, moving weights, gyrostabilisers and zero-speed fin stabilizers [4, Wang et al, 2009], [5, Liang et al., 2015]. Zero speed fin stabilizer is created based on the improvement of conventional fin stabilizer. It can achieve good roll reduction not only at high speed, but also at low/medium and zero speed. Zero-speed fin stabilizer produces righting moment to damp ship's roll motion through actuation of controlled hydrofoils. Both the aspect ratio and the distance between the shaft and the leading edge are smaller than the traditional fin stabilizers and it requires larger driving power than conventional fin stabilizers. Except for the above conventional devices, the research on new types of roll damping equipment, for instance the rotating roll stabilizer, is ongoing. It generates lift based on Magnus effect through the rotating rotor wing mounted on the side of the hull to reduce ship's roll motion. On the other hand, in order to design new roll stabilization

devices, it is also carried out lots of studies and tests on the anti-rolling mechanism of zero - speed fin stabilizer, which provides theory references for its practical application.

The anti-rolling tank generates restoring torque through water's reciprocating motion. It takes up valuable space in the cabin to achieve the roll reduction effect [6, Liang et al,2012]. Similar to anti-rolling tank, moving weights reduce ship's roll motion by controlling the movement of the weights. It requires large power consumption [7, Lewis, 1989]. Gyrostabiliser generates stabilization torque to oppose the dynamic wave-induced rolling motion through the combination of the angular momentum of the spinning flywheel and the flywheel's precession oscillation [8, Perez, 2005].

The other direction is the study on new types of roll stabilization equipment. Rotating roll stabilizer based on Magnus effect, the sideways force on a translating and rotating sphere or cylinder, is discussed in several fluid dynamics textbooks [9]-[11], but confusion can occur when it is combined with other effects, such as friction and eddy forming or shedding. In the case of either rapid spinning or rapid translation or both, the extraneous effects of friction and eddy shedding would be relatively more important. Possible deficiencies in the existing literature can be addressed by adapting rotation to a new formulation of the flow past a cylinder that is not founded on the usual assumption of irrotationality [12]. The pressure and velocity fields surrounding the cylinder can both be specified.

Researchers have been trying to apply the lift generating mechanism of Magnus effect [13] into practice since Prandtl [14] proposed the maximum lift coefficient can reach 4π. In 1852, the German physicist and chemist, Heinrich Gustav Magnus (1802–1870), made experimental studies of the aerodynamic forces on spinning spheres and cylinders (The effect had already been mentioned by Newton in 1672, apparently in regard to spheres or tennis balls). These experiments led to the discovery of the Magnus Effect, which helps explain the theory of lift. So far, it has been applied to aeronautics [15], wind turbines [16], ship industry such as propulsion assisted [17], rotating cylinder rudder [18] and rotating roll stabilizer. The world's first rotating roll stabilizer based on Magnus effect was designed by Theo Koop in 1980. It was installed in a small boat and proved to be effective in roll reduction. It is not until the recent decades that Magnus rotating roll stabilizers have seen practical application with the development of sealing and control technologies. The world's first electrical Magnus effect yacht stabilizer system was created by Rotor Swing Marine and it has a good roll damping performance at low speed. The similar product of Quantum Control with the brand name MagliftTM system is driven by hydraulic system which makes it suitable for large yachts and research vessels.

In this study, flow around the rotating cylinder, which is an important component in the design of Magnus effect roll stabilizer system was investigated. Formation of the Magnus lift force depending on the cylinder rotation speed was observed at two different fluid speeds for the cylinder with fixed length. Magnus lift force were calculated numerically and experimentally, depending on the variation of cylinder rotational speeds at 1,2 m/s and 1,72 m/s fluid speeds.

Working principles of Magnus effect roll stabilizer system was explained in Section 2. Theoritical framework were investigated in section 3. Numerical studies on cylinder at different rotatiaonal speeds have been shown in Section 3. Information about the experimental studies is given in Section 4. Results from numerical calculation and experimental studies were calculated in Section 5. The conclusions and recommendations of the study are given in Section 6

2. Modeling of Rotating Roll Stabilizer System

According to ship motions, large amplitudes and dynamic accelerations can cause passengers on board to depict motion sickness symptoms and thereafter the crew-induced errors. Therefore, anti-rolling systems are of great importance for damping the roll motion in ships and marine structures. The

Magnus principle is one of the anti-rolling systems that a circular cross-sectional rotor system rotates around its longitudinal axis to generate Magnus force.

The basis of the investigation of the flow around the rotating cylinder is based on studies on various Reynold numbers [14]. Vortex shedding was observed in the case of $\alpha < 1.91$ and high spin ratios (*the circumferential velocity of the cylinder, V_θ/ the free-stream velocity, V_∞*) led to achievement of higher Magnus lift coefficients with different α, from 0 to 5 at Re = 200 for 2D rotating cylinder [20, Mittal and Kumar (2003); 21, Mittal (2004)].

Mittal (2004) also performed 3D numerical case of Re = 200 and $\alpha = 5$ in order to observe the instabilities in wake region. Experimental and numerical studies of the flow around the rotating cylinder indicated that the three-dimensional effects bring the mean lift force measured at a given rotational speed below the level obtained in the two-dimensional flow. The wake formation behind the rotating cylinder within a certain Re and α range was strong under conditions where the α is less than 1, and it was suppressed around $\alpha = 2$ at $Re = 9 \times 10^3$ [22, Doll et al. (2008)]. Aljure et al. (2015) examined the Strouhal number, lift force and the behavior of the separation point using Direct Numerical Simulation (DNS) in the range $0 < \alpha < 5$ and $Re = 5 \times 10^3$ and the vortex shedding occurred in cases where $\alpha < 2$. The increase in 'α' caused the average drag force to decrease while the lift force to increase. Karabelas (2012) stated that the spin ratio affects the turbulent flow profile with high-Reynolds numbers differs from the laminar regime. The 2D simulations solved with the k-ε turbulence model using α ranging 2 to 8 and the high Reynolds numbers, $Re = 5 \times 10^6$, 1×10^6 and 5×10^6.

The flow past rotating cylinder using different RANS turbulence models and using a 2D discrete vortex simulation method was studied and observed the development of negative Magnus force within $0 < \alpha < 19$ and $Re = 10^5 - 1.3 \times 10^5$. The vortex shedding disappeared at $\alpha \approx 3.5$, and the lift coefficient results exceeded the Prandtl's limit [25, Dasgupta et al. (2020); 26, Chen et al. (2020)].

The hydrodynamic characteristics of Magnus stabilizer system investigated experimentally in term of the effects of roughness and rotation speed in the range of $2.3 \times 10^4 < Re < 1.4 \times 10^5$ and $0 < \alpha < 3.5$. It was stated that the Magnus stabilizer system provided better performance at lower ship speeds and the lift and drag characteristics had a minor dependency on Reynolds number at certain intervals of the spin ratio [27, Sosa (2014); 28, Sosa and Ooms (2016)]. It is also performed the numerical simulations of 3D cylinder in low free stream velocity, and worked on a PID controller mechanism to investigate the anti-rolling effect with the rotational speed changing from 300 RPM to 1500 RPM in the range of $4.7 \times 10^5 < Re < 2.6 \times 10^6$ [29, Liang et al. (2016)].

2.1. Analysis of Anti-Rolling Mechanism

As shown in Figure 1, the rotor wing is rotating clockwise in a streaming fluid from left to right. According to the non-slip condition, the fluid layer around the surface of rotor wing will move as its rotation, which boosts the velocity of the fluid stream in the direction of rotation and opposes it in the reverse direction. That is, the velocity of the flow around the upward surface is faster than that around the downward surface.

According to Bernoulli's equation that higher velocity means lower pressure, the pressure of the upward surface of the rotor wing is lower than that of the downward surface. The difference of the pressure between the upward surface and the downward surface leads to an upward force perpendicular to the axis of rotation and the direction of the streaming fluid. This phenomenon is the famous Magnus effect [13]. The Magnus effect is a concept of fluid dynamics that is the result of spinning spheres or cylinders

moving forward through a fluid. It is described by the surface of the sphere or cylinder pulling the fluid around, either a sphere or cylinder, in the direction of the spin. Once reaching the side opposite of the cylinder, the fluid separates from the surface of the object and continues in a linear direction tangent from the cylinder (see Figure 1). Newton's Third Law states that for every action, there is an equal and opposite reaction, so when the sphere or cylinder forces the fluid around, and it separates going in a tangent direction, then a force put onto the object in the opposite direction.

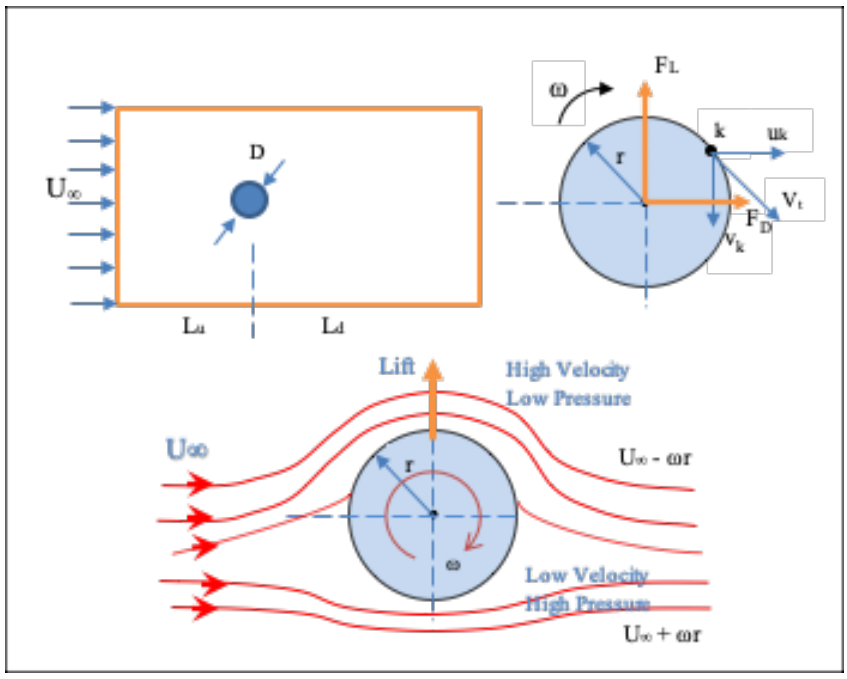

Figure 1: Generation of Magnus lift force around the rotating cylinder

Figure 1 depicts the rectangular computational domain used in the numerical simulations that follows, and illustrates the components of the velocity imposed over each Lagrangean point k, obtained by decomposing the tangential velocity $U_t = \omega r$. The domain was set to be L_u and L_d in the streamwise direction and D is the diameter of the cylinder located inside the computational domain.

The boundary conditions adopted for the velocity are: inlet: u = U and v = 0; outlet: $\partial u / \partial x = \partial v / \partial x = 0$; top and bottom: $\partial u / \partial y = \partial v / \partial y = 0$. For the pressure, the Newmann conditions in the inlet ($\partial p / \partial x = 0$), and the Dirichlet conditions in the outlet, top and bottom (p = 0), were assumed.

3. Theoretical Framework

First, a formula for the Magnus force can be constructed from information already available. Consider uniform frictionless horizontal flow of magnitude 'U' moving from left to right past a cylinder of radius 'r'. The cylinder is not rotating on its axis. Pressure, drag and lift for uniform flow over a cylinder as follows:

$$\psi = u.r.sin\theta.\left[1 - \frac{a^2}{r^2}\right] \quad (1)$$

Where, ψ represent the stream function and r = a along the cylinder surface. If appropriate derivative operations are applied on the stream function, u_r (radial velocity) and u_Θ (angular velocity) components of velocity are obtained.

$$u_r = \frac{1}{r}\frac{\partial \psi}{\partial \Theta} = u\,.\,cos\Theta\,.\left[1-\frac{a^2}{r^2}\right] \tag{2}$$

$$u_\Theta = -\frac{\partial \psi}{\partial r} = -u.\,sin\Theta.\left[1+\frac{a^2}{r^2}\right] \tag{3}$$

The velocity components become for r = a ; $u_r = 0$ and $u_\Theta = -2u.sin\Theta$; u_Θ is maximum at $\theta = \pi/2$ and $3\pi/2$; zero at $\theta = 0$ and $\theta = \pi$. The pressure distribution can be obtained using Bernoulli's Equation: p_0 is the pressure of free stream velocity and p_s is the pressure on the cylinder surface.

$$p_0 + \frac{1}{2}\rho u^2 = p_s + \frac{1}{2}\rho {u_\Theta}^2 \tag{4}$$

$$p_s - p_0 = \frac{1}{2}\rho u^2(1-4sin^2\Theta)$$

$$C_p = (1-4sin^2\Theta) = (p_s - p_0)/(0{,}5.\rho u^2) \tag{5}$$

C_p is the dimensionless pressure coefficient. The drag on the cylinder, F_D may be calculated through integration of the pressure cosine component over the cylinder surface;

$$F_D = -\int_0^{2\pi} p_s \cos\theta \cdot a d\theta = -\int_0^{2\pi}[p_0 + 0.5\rho u^2(1-4\sin^2\theta)]\cos\theta \cdot a d\theta \tag{6}$$

The drag on the cylinder acts parallel to the flow. On the other hand, the lift is perpendicular to the flow.

$$F_L = -\int_0^{2\pi} p_s \sin\theta \cdot a d\theta = -\int_0^{2\pi}[p_0 + 0.5\rho u^2(1-4\sin^2\theta)]\sin\theta \cdot a d\theta \tag{7}$$

The maximum horizontal speed U_∞ comes from the irrotational solution for flow past a cylinder. The acceleration of gravity does not appear; it has no bearing on what follows. Next, let the cylinder rotate counter-clockwise with constant angular frequency ω. Pressure, drag and lift for uniform flow over a rotating cylinder as follows:

$$\phi = u.r.cos\Theta.\left[1+\frac{a^2}{r^2}\right] - \frac{\Gamma}{2\pi}\Theta \tag{8}$$

$$\psi = u.r.sin\Theta.\left[1-\frac{a^2}{r^2}\right] + \frac{\Gamma}{2\pi} ln(r) \tag{9}$$

In the equation (8) and (9); ϕ reperesents the potantial function, ψ represent the stream function and Γ represent the circulation. Thus velocity componenets u_r and u_Θ of rotating cylinder can be written as equation (10) and (11).

$$u_r = \frac{\partial \phi}{\partial r} = u.cos\Theta.\left[1 - \frac{a^2}{r^2}\right] \tag{10}$$

$$u_\Theta = \frac{\partial \phi}{\partial \Theta} = -u.sin\Theta.\left[1 + \frac{a^2}{r^2}\right] - \frac{\Gamma}{2\pi r} \tag{11}$$

r = a along the cylinder surface so velocity components become; $u_r = 0$ and $u_\Theta = -2u.sin\Theta - (\Gamma/2\pi r)$. The pressure distribution arounde the rotating cylinder can be obtained using Bernoulli's Equation.

$$p_0 + \frac{1}{2}\rho u^2 = p_s + \frac{1}{2}\rho {u_\Theta}^2 \implies p_s - p_0 = \frac{1}{2}\rho(u^2 - {u_\Theta}^2) \tag{12}$$

Equation (13) is obtained if the expressions in equation (10) and (11) are substituted for the velocity components in equation (12). If equation (13) is integrated along the cylinder surface, the lift force generated around the rotating cylinder in the fluid field is found.

$$p_s - p_0 = \frac{1}{2}\rho u^2(1 - 4sin^2\Theta - \frac{2.sin\Theta.\Gamma}{\pi.a.u} - \frac{\Gamma^2}{4.\pi^2.a^2.u^2}) \tag{13}$$

$$F_L = \int_0^{2\pi} p_s.sin\Theta.d\Theta = \rho u\Gamma \tag{14}$$

$$F_D = \int_0^{2\pi} p_s.cos\Theta.d\Theta = 0 \tag{15}$$

In the nonviscous fluid no drag for a rotating cylinder and there is a lift proportional to density, upstream velocity and strength of vortex. Thus, lifting effect for rotating cylinder in a free stream is called Magnus Effect. Pressure at top of the cylinder P_T and pressure at the bottom of cylinder P_B are expressed by equation (16) and (17).

$$p_T = const. - \frac{1}{2}\rho(U + \omega r)^2 \tag{16}$$

$$p_B = const. - \frac{1}{2}\rho(U - \omega r)^2 \tag{17}$$

Assume for simplicity that the magnitude of U is greater than the magnitude of ωr. Between the top and the bottom the pressure difference is expressed by equation (18).

$$p_T - p_B = -2\rho U\omega r \tag{18}$$

And the pressure gradient across the cylinder is shown by equation (19).

$$\frac{p_T - p_B}{2r} = \rho U \omega \tag{19}$$

Pressure is lower on top of the cylinder due to increasing the velocity; the pressure force points up. Equation (19) gives the irrotational pressure force (Magnus force) on the cylinder along the vertical line passing through the cylinder's center. In general the speed and the frequency in equation (19) are independent variables (for rolling motion they are related).

Begin again with a steady frictionless flow, from left to right, past a cylinder that is not rotating. Far from the cylinder the velocity of the fluid is constant in magnitude, *U*, and uniform in direction, but this time no irrotational assumption is made. Normal to the mean flow and at the top of the cylinder the z-axis points up. In this two-dimensional problem the flow around the cylinder cross-section is in the x-z plane, and the long axis of the cylinder is in the y-direction.

The Bernoulli equation states that the total pressure is a constant along the streamline. So, as the top part of the cylinder is working with the uniform flow and creating the faster velocities and against the flow creates slower velocities, the pressures are different. With a higher velocity at the top, it can be concluded that the pressure at the top of the cylinder must be lower, and the pressure at the bottom of the cylinder must be higher (Figure 1).

Bernoulli's equation along any streamline going over the top of the cylinder is expressed by equation (20).

$$p = const - \rho . g . z - \frac{1}{2}\rho U^2 \tag{20}$$

Where p is the pressure, U is the speed of the flow and ρ is the fluid density, taken constant and g is the acceleration due to gravity. The Bernoulli's Equation expresses conservation of energy and assumes that there is no friction and the fluid is no viscous and incompressible. For ease of calculation the constant in (20) is assumed the same for all streamlines.

Fluid following a curving path anywhere above the top of the cylinder experiences an upward centrifugal force which attempts to tear the fluid away from the solid and away from itself. When the flow is steady, as often observed at low speeds, there must be an equal but opposite force to balance the centrifugal force everywhere. It can only be a pressure gradient in this situation. Therefore the force balance can be shown like equation (21).

$$\frac{dp}{dz} = \frac{\rho . U^2}{R} \tag{21}$$

In equation (21) R is the radius of curvature of the streamlines, which is the same as the radius of the cylinder at the top of the cylinder. Adopting the convention that R is positive, then the right hand side of equation (21) is positive. Thus the left hand side of equation (21) shows that the pressure must increase with increasing height over the cylinder, or that the perturbed pressure (the relatively low pressure at the cylinder's top) decreases upward.

Now, between equation (20) and equation (21) the pressure can be eliminated quickly, starting by taking the z derivative of both sides of equation (20), substituting the pressure gradient from it into the pressure gradient in equation (21), to form a velocity equation for variations in the z-direction.

$$\frac{dU}{dz} = -\frac{U}{R} \tag{22}$$

Equation (22) is a first order ordinary differential equation with a non-constant coefficient, since $R = R(z)$ above the cylinder. Unlike either one of the two equations it came from Equation (22) is linear. However, in order to solve (22) completely information has to be provided about the radius of curvature of the streamlines. Observations show that the radius of curvature of the streamlines above the top of a cylinder increases with increasing distance away from the cylinder until, only a few radius away, there is no longer any curvature left (the streamlines are straight). It is not obvious from the available data what the exact rate of increase is, although one might be able to say that the increase is faster than linear. Also a principle of physics does not occur at this time that could help determine the explicit rate of increase algebraically. Whatever the true vertical structure of the radius of curvature of the streamlines turns out to be, Equation (22) can be solved, if not analytically, then numerically, since only a first order ordinary differential equation needs to be deal with.

3.1 Working mechanism of rotating roll stabilizer

The lift on a rotating rotor wing in a streaming fluid can be calculated based on Kutta-Joukowski theorem [9]. Kutta-Joukowski theorem gives the relation between lift and circulation on a body moving at constant speed in a real fluid with some constant density. The Kutta-Joukowski Lift Theorem defines the behavior of a cylinder spinning on its longitudinal axis, per unit length, considering the density of the fluid being traveled through, velocity which it is traveling through the fluid, and the vortex strength based on the radius of the cylinder and angular velocity. It is based on the same principle as the Magnus Effect except applied to a three dimensional cylinder, rather than a theoretical circular object. Applied, it functions off mostly the concepts of the Magnus Effect (Newton's Third Law) for lift, but also touches on the force of lift created by Bernoulli's principle, though it is not a major contributor to its force of lift.

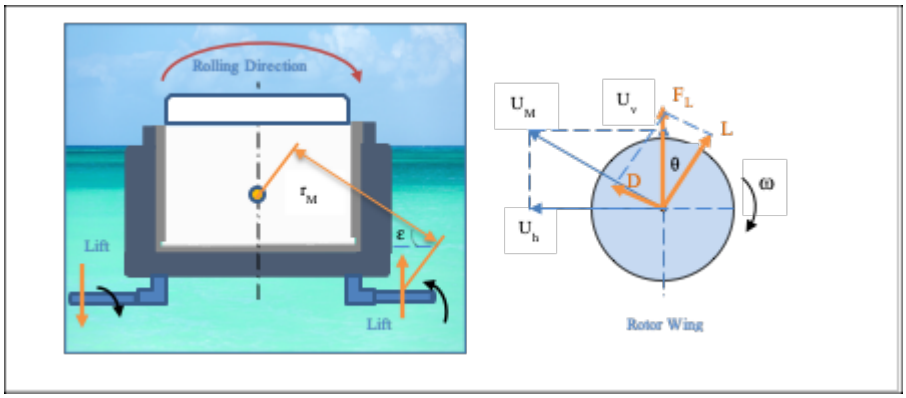

Figure 2: Roll damping mechanism of Magnus rotor wing.

In Figure 2, the vertical component of the fluid flow caused by ship roll motion can not be omitted in lift calculation. The lift taken into account by the controller should comprise both components of the fluid flow the vertical and the horizontal one. The directions of the fluid flow, the rotation and the force of the rotor wing are shown in Figure 2. $U_h = U$ is the horizontal velocity caused by ship speed. $V_v = r_\omega \dot{\phi}$ is the vertical velocity caused by ship's roll motion (ϕ is the roll angle). $r_\omega = r_M \cos\varepsilon$ is the roll arm of Magnus rotor wing. r_M represents the distance between the hydrodynamic pressure-center and the center of gravity of the ship. ε is the included angle between r_M and the horizontal base line. U_M is the resultant velocity of U_H and U_V. L and D are the lift and drag cause by U_M. ω is the rotation speed of the rotor wing. F_L is the force used to stabilize ship's roll motion as follows:

$$F_{magnus} = \rho . U . L . \Gamma \tag{23}$$

Where ρ is the density of the streaming fluid, U 'is the velocity of the streaming fluid, L is the length of the cylinder, Γ stands for the circulation of the cylinder, which is a line integral (around a closed loop, enclosing surface of the body) of the tangential velocities along the loop and results from equation (24).

$$\Gamma = \oint U_t . ds \tag{24}$$

Where $U_t = r.\omega$ represents the rotational speed, angular velocity $\omega = (2\pi n)/60$, n is the rotation number in per minute. Thus, if equation (24) is arranged general formula of circulation is obtained like equation (25).

$$\Gamma = 2\pi . r^2 . \omega \tag{25}$$

where r is the radius of the rotor wing and ω is the angular velocity of spin of the cylinder. For convenience, the equation (26) can be wrote.

$$F_{magnus} = K . \omega . U \tag{26}$$

where K is the proportional coefficient and it can be regarded as a constant if the cylinder and the streaming fluid are confirmed.

$$K = 2\pi . r^2 . \rho . L \tag{27}$$

It can be concluded that the lift is proportional to the rotational speed of the cylinder and the velocity of the streaming fluid, as shown in equation (27). The direction of Magnus lift depends on both the direction of streaming flow and cylinder's rotational direction. The Magnus lift is related to the length, the radius, the rotation speed of the rotor wing and the density, the velocity of the streaming fluid. It is proportional to the rotor's rotational speed when the rotor size, fluid density and velocity are confirmed.

The Magnus lift coefficient C_L is non-dimensionalized in 2D by the quantities where ρ is the density of fluid, D is the cylinder diameter,

$$C_L = \frac{F_L}{0{,}5.\rho.D.U_\infty^2} \tag{28}$$

The formulas above are calculated under ideal conditions, while the fluid in real world is viscous. The pressure distribution of the rotor wing surface is influenced by ocean environment, ship hull, friction loss, vortex turbulence as well as boundary-layer separation. All of those lead to the realistic Magnus lift is smaller than that of the theoretical value. As shown in Figure 2, the rotor wing of the right side is rotating clockwise while the left one is rotating counterclockwise if we see it from right to left. According to the analyses above, it is easy to find out that the lift on the right rotor wing is upward while the left one is downward relative to the direction of the fluid. The anti-rolling torque is achieved relative to the ship roll axis to resist interfering moment and reduce ship roll motion. This is right the stabilization mechanism of Magnus rotor wing.

4. Numerical methodology

With the increase in the Reynolds number in a flow field, laminar flow regime changes to the turbulent flow regime. The fluid velocity will increase around the rotating cylinder in the flow field. For this reason, turbulence will be observed around the rotating cylinder. In order to calculate the Magnus lift force correctly with numerical methods, the turbulence model must be included in the calculations. In CFD analysis, two different turbulence models are suggested depending on the Reynolds number. *k-w,* model is recommended for low Reynolds number values and *k-ε* model is recommended for high Reynolds number values. Depending on the parameters we examined within the scope of the article, the *k-w* method will be used in numerical calculations.

The dimensionless wall distance, *y+* value, is an important parameter to consider when modeling the mesh. With the rotation of the cylinder, the current will accelerate in the region close to the cylinder. In order to achieve the correct result in numerical calculation, a suitable mesh model should be created around the cylinder according to the *y+* value. [30, Tu et al. (2018)] showed that taking the value of 1 for *y+* in the fluid field with low Reynolds number gives correct results. According to the determined *y+* value, the height of the first mesh on the cylinder surface is calculated. The mesh around the cylinder will be modeled as layers of circular cross section. Each layer will be 1,2 times the previous one and will continue to expand. The remainder of the fluid field will be modeled with a rectangular mesh. The region close to the cylinder surface is modeled with a dense mesh, and the mesh becomes sparse as it moves away from the cylinder surface (see Figure 3, Figure 4, Figure 5).

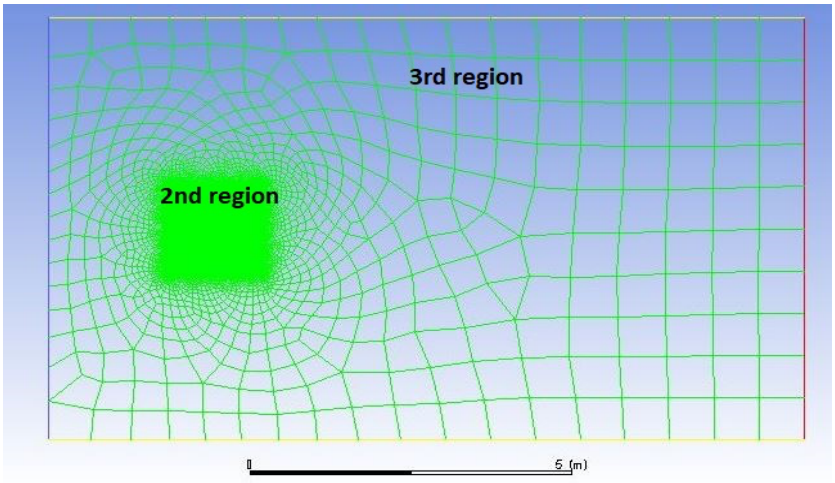

Figure 3: Overall mesh domain

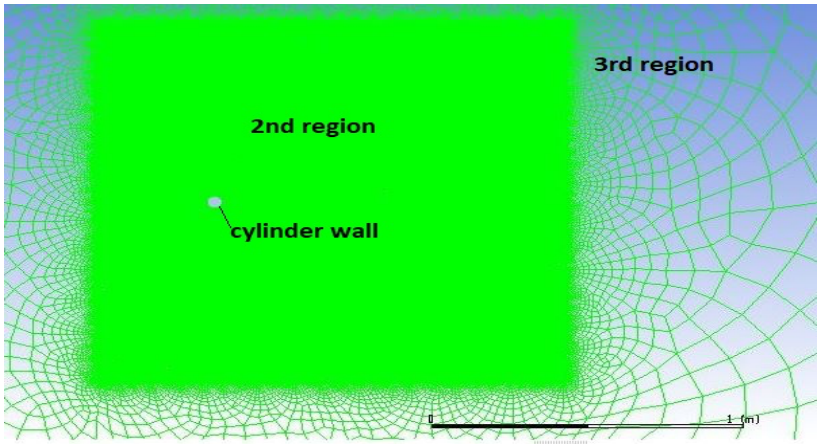

Figure 4: Mesh model of the region close to the cylinder wall

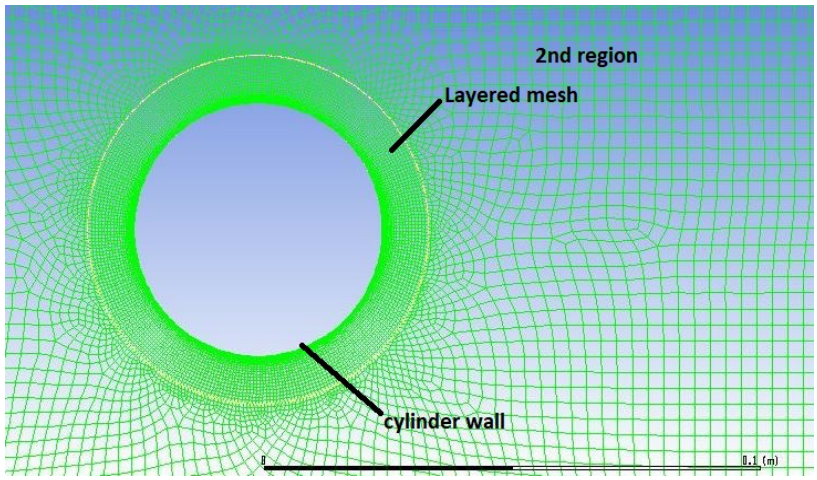

Figure 5: Layered mesh model around the cylinde

Numerical analyses were performed for velocities of 1.2 m/s and 1.72 m/s. The cylinders were rotated at speeds of 800 rpm – 1600 rpm at these flow rates. Velocity and pressure of flow characteristics in each analysis are shown in the following images (Figure 6, Figure 7, Figure 8, Figure 9, Figure 10, Figure 11, Figure 12, Figure 13, Figure 14, Figure 15).

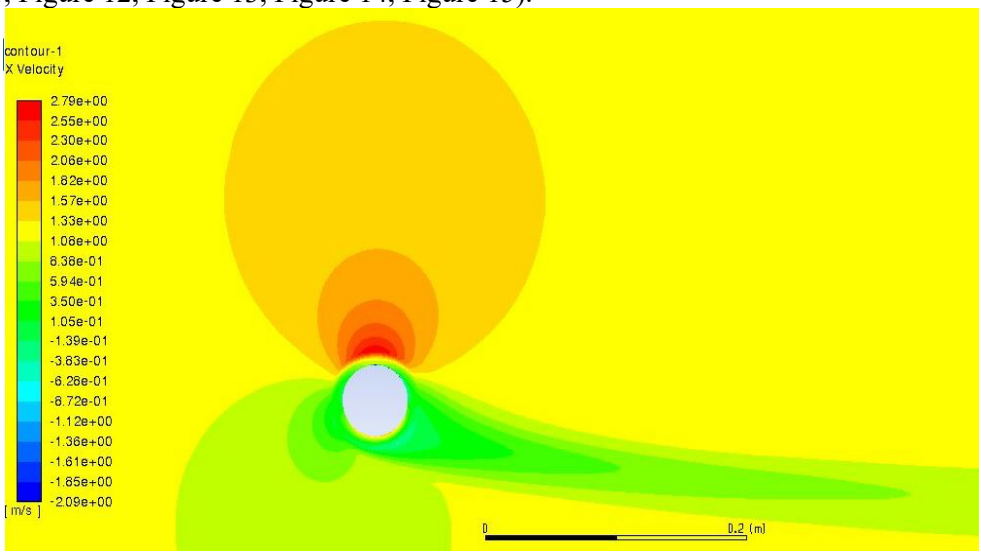

Figure 6: x velocity at v=1.2 m/s - 800 rpm.

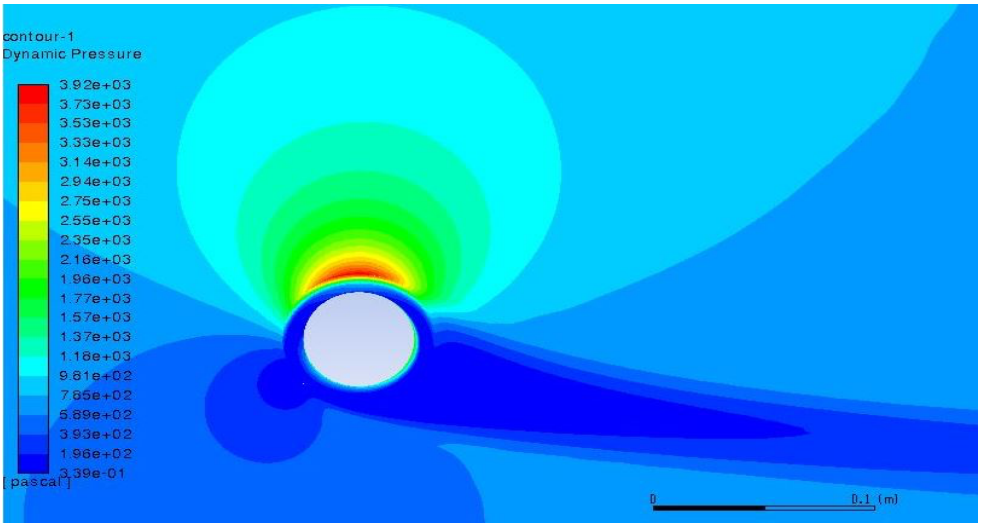

Figure 7: pressure at v=1.2 m/s - 800 rpm.

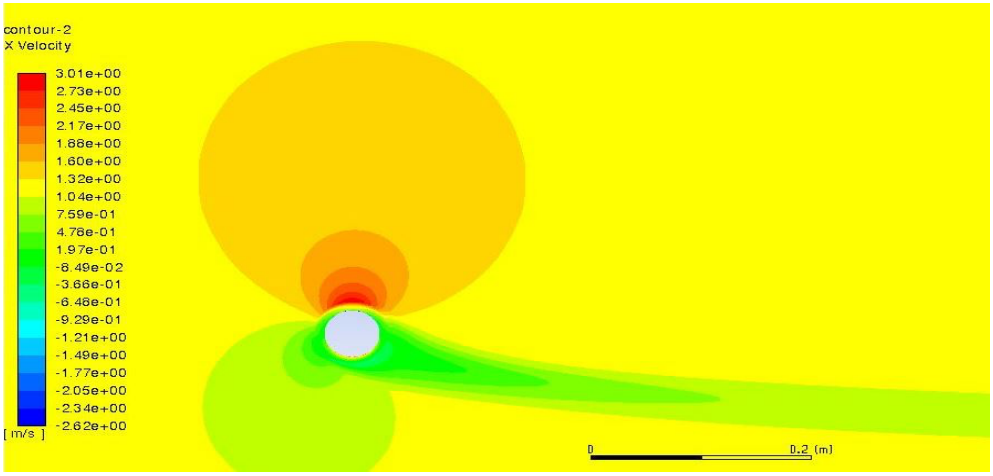

Figure 8: x velocity at v=1.2 m/s - 1000 rpm.

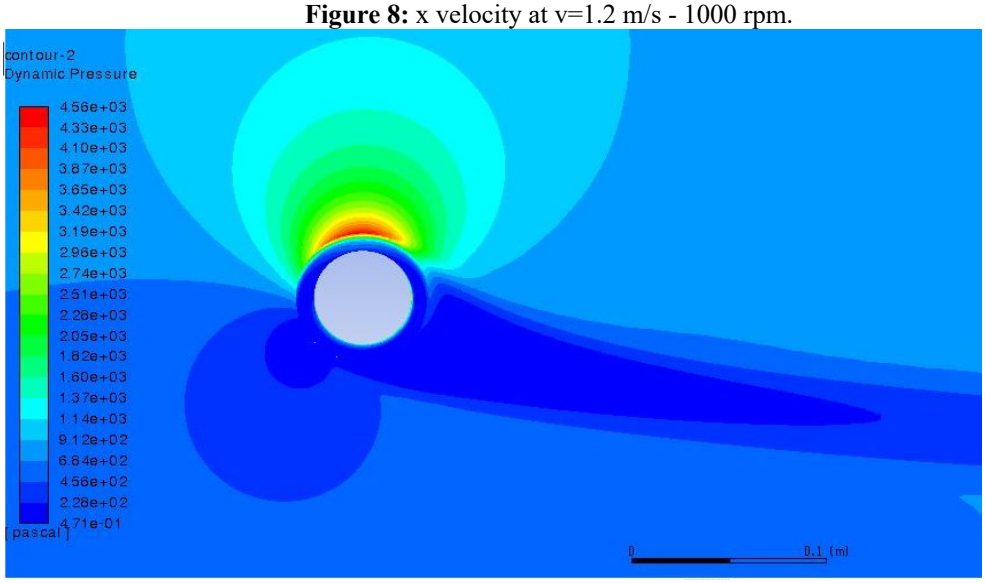

Figure 9: pressure at v=1.2 m/s - 1000 rpm.

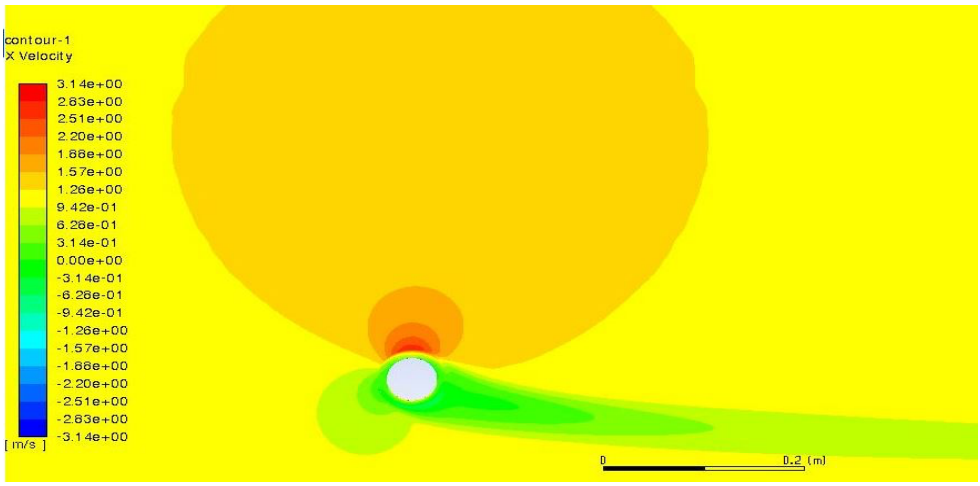

Figure 10: x velocity at v=1.2 m/s - 1200 rpm

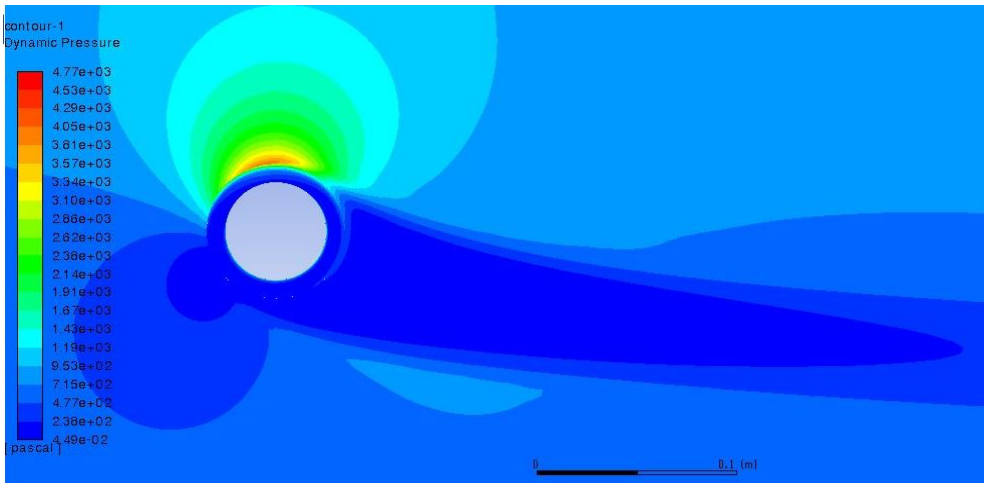

Figure 11: pressure at v=1.2 m/s - 1200 rpm.

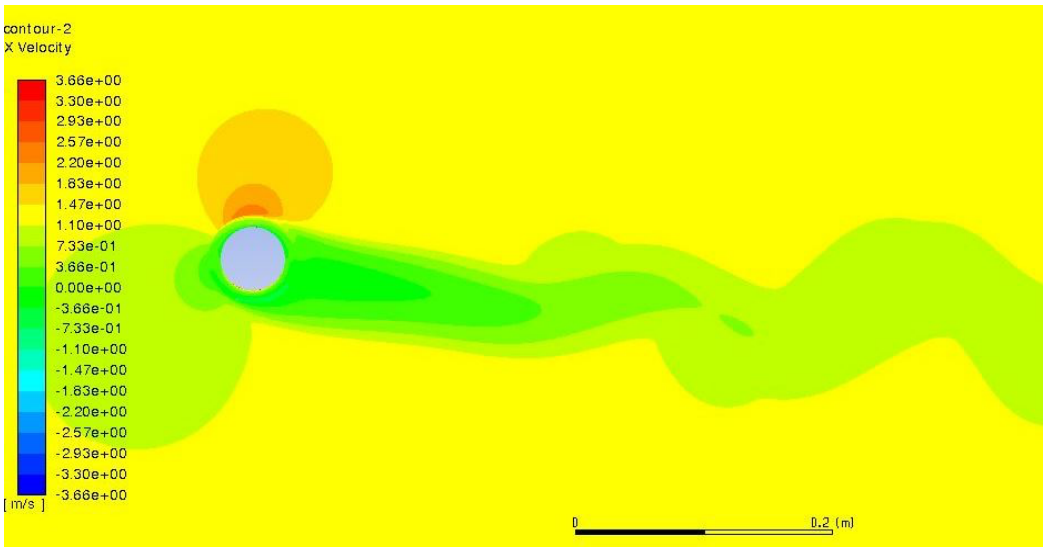

Figure 12: x velocity at v=1.2 m/s - 1400 rpm.

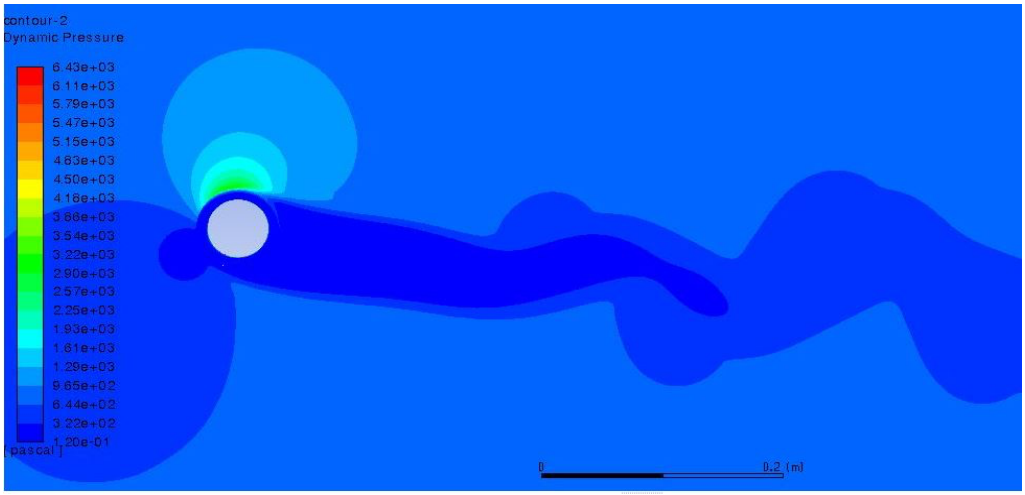

Figure 13: pressure at v=1.2 m/s - 1400 rpm.

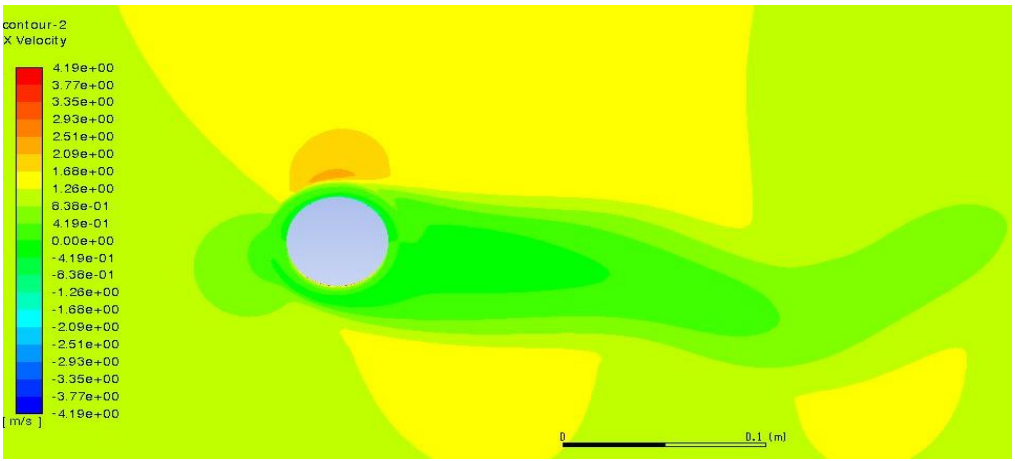

Figure 14: x velocity at v=1.2 m/s - 1600 rpm.

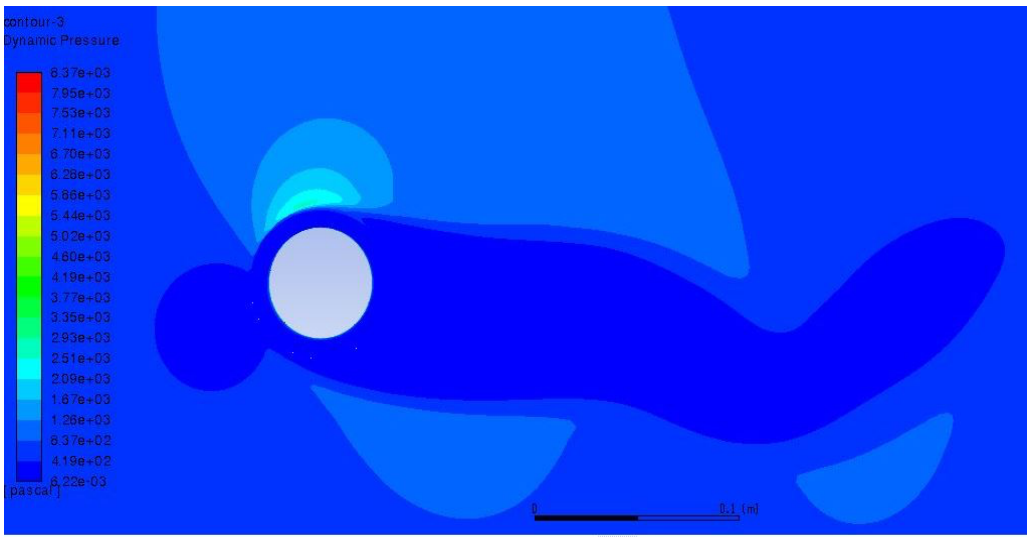

Figure 15: pressure at v=1.2 m/s - 1600 rpm.

A linear increase in pressure and velocity values was observed when the revolution speed was increased from 800 rpm to 1200 rpm. From the CFD analysis graphs, it was observed that there was no increase in the pressure value after 1400 rpm. After this value, an increase in cylinder rotation speed will not cause an increase in lifting force. In velocity fields, oscillations are observed after 1400 rpm (see Figure 12, Figure 13, Figure 14, Figure 15). It is understood from the CFD analysis that 1400 rpm is a critical value for the design of the roll stabilizing system. The cylinders will not need to be rotated at more than 1400 rpm at 1,2 m/s fluid speed. The system will operate in the most efficient way by changing the direction of rotation of the cylinders depending on the period of the boat at the specified rotation speed. In order to observe the effect of fluid velocity on velocity and pressure fields, analyzes were performed at the same cylinder rotational speeds at a fluid velocity of 1.72 m/s. A proportional increase in velocity and pressure values was observed with the increase of fluid velocity.

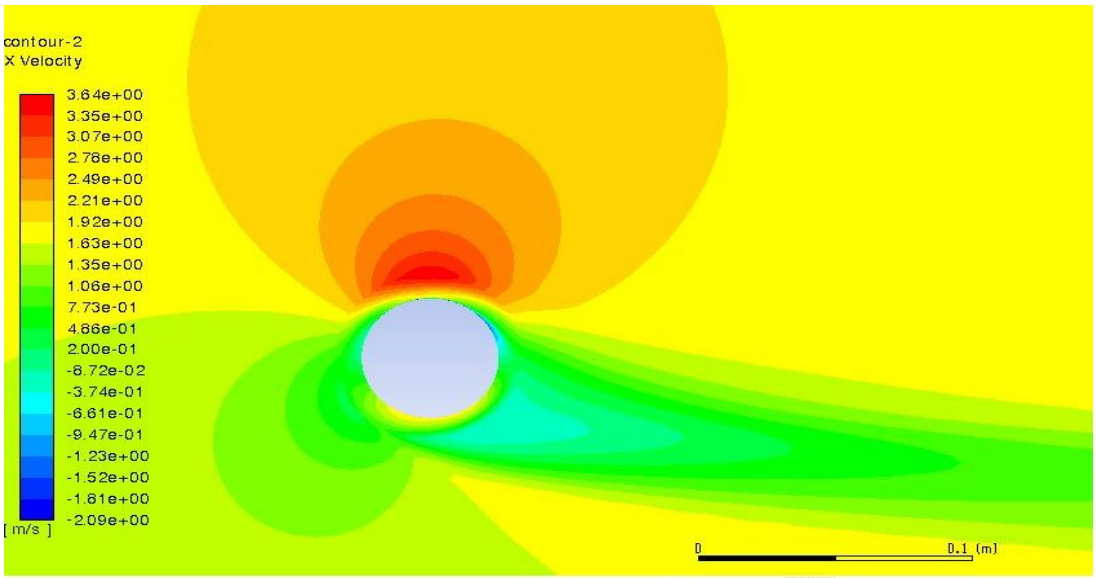

Figure 16: x velocity at v=1.72 m/s - 800 rpm.

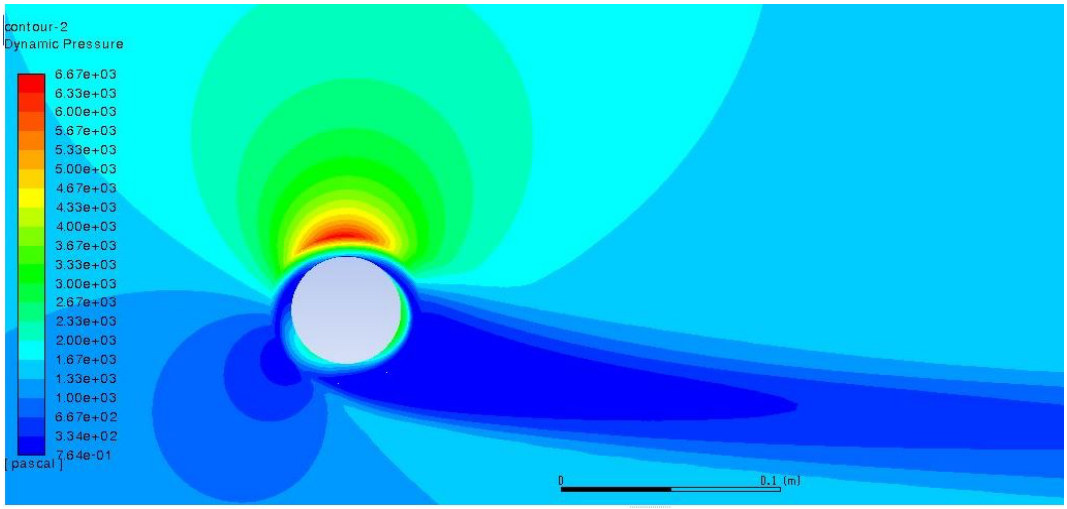

Figure 17: pressure at v=1.72 m/s - 800 rpm.

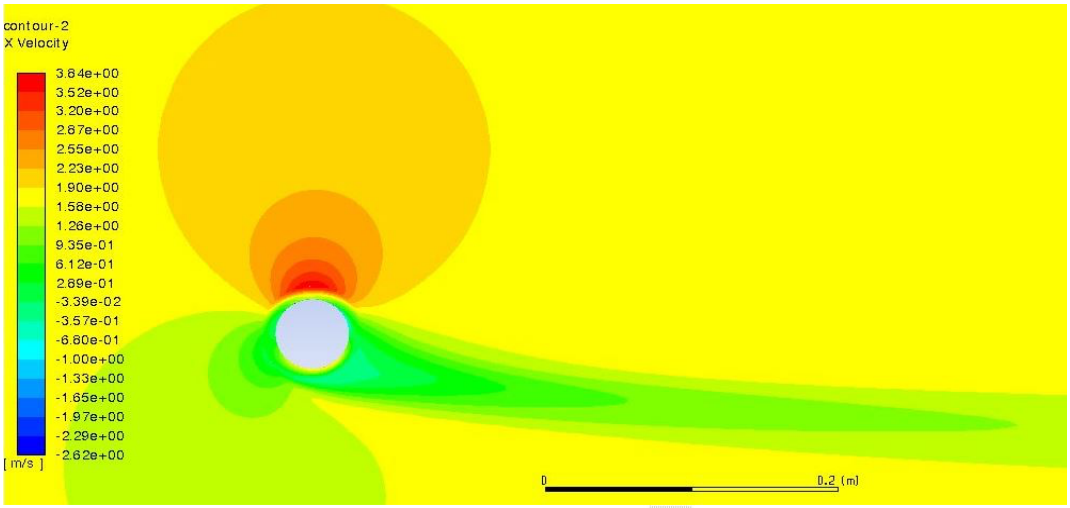

Figure 18: x velocity at v=1.72 m/s - 1000 rpm.

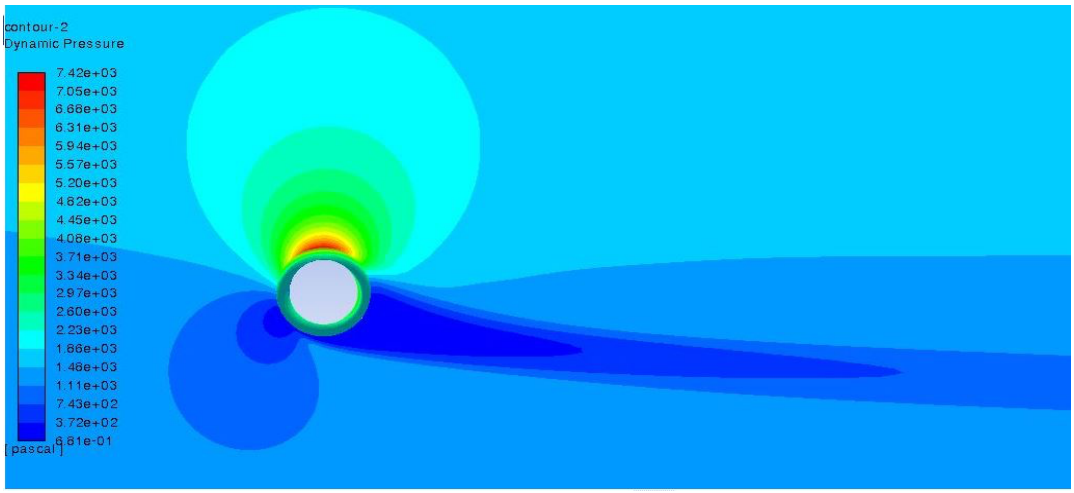

Figure 19: pressure at v=1.72 m/s - 1000 rpm.

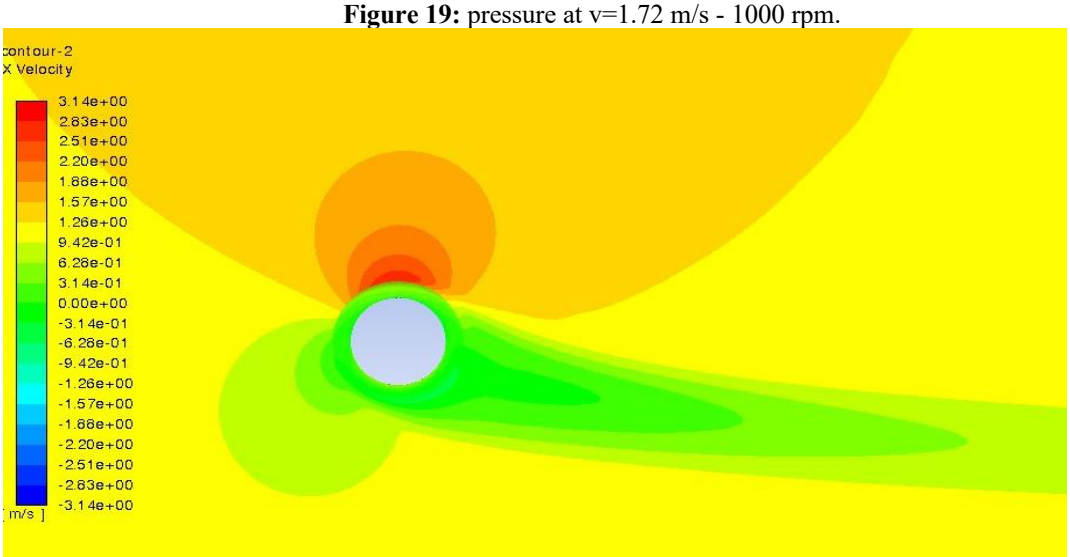

Figure 20: x velocity at v=1.72 m/s – 1200 rpm.

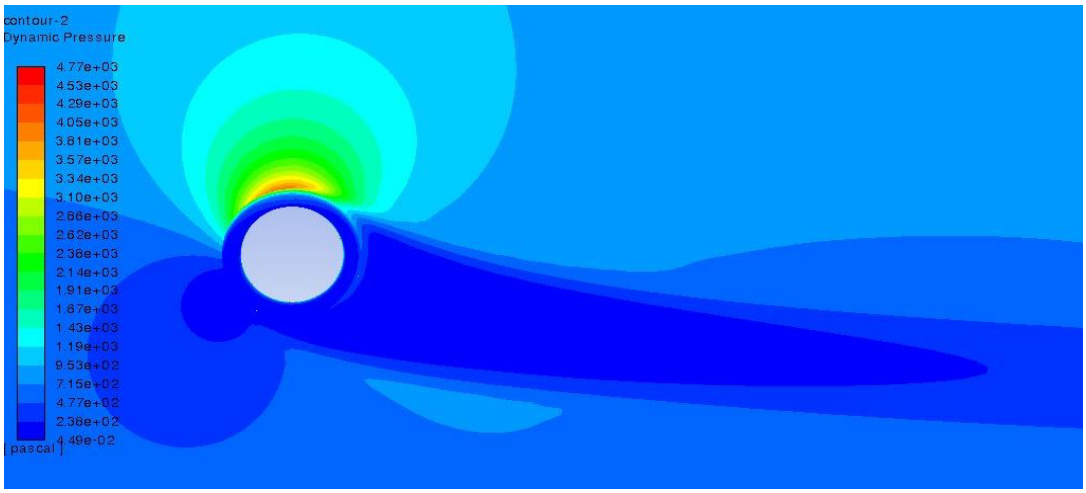

Figure 21: pressure at v=1.72 m/s - 1200 rpm.

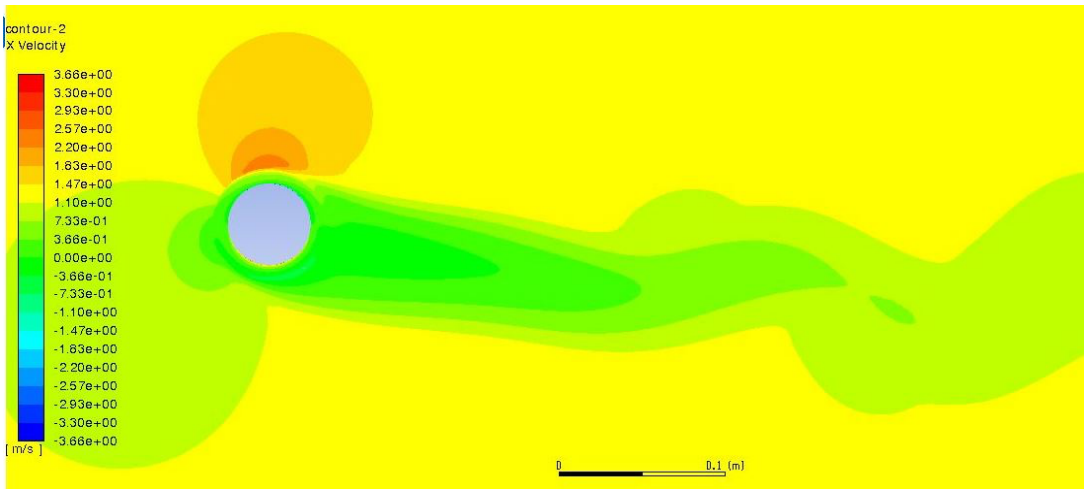

Figure 22: x velocity at v=1.72 m/s – 1400 rpm

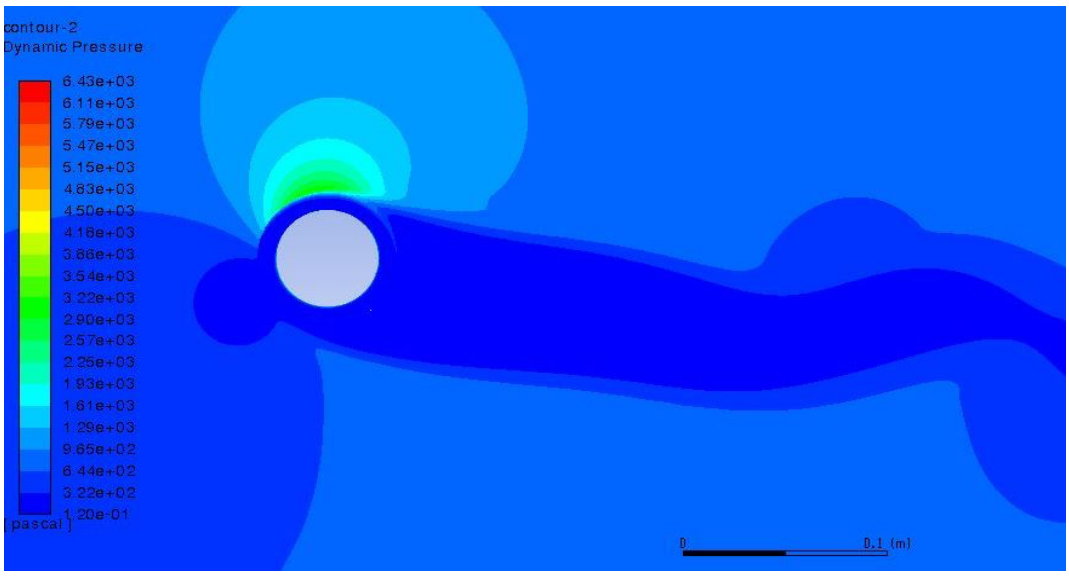

Figure 23: pressure at v=1.72 m/s - 1400 rpm.

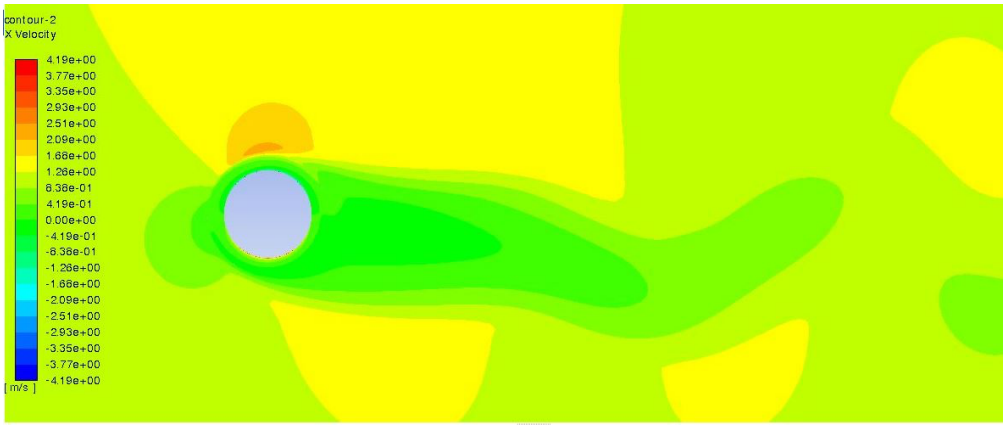

Figure 24: x velocity at v=1.72 m/s – 1600 rpm.

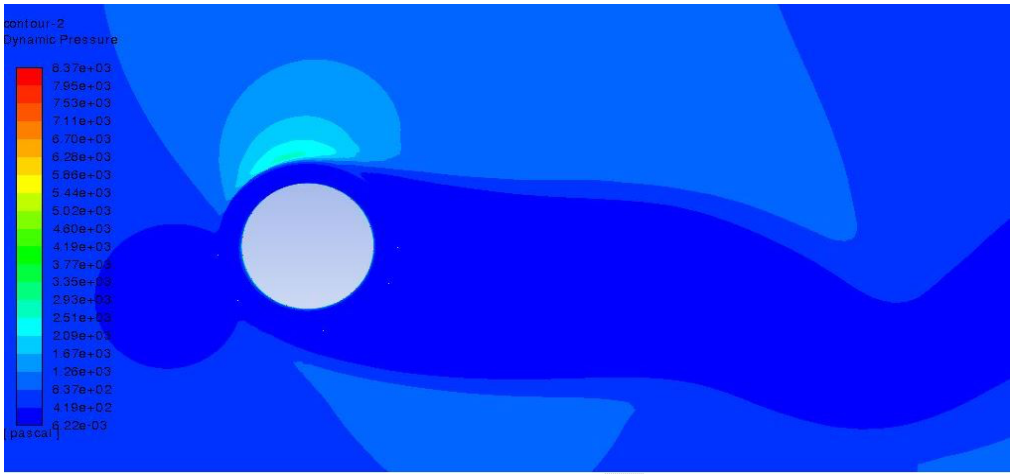

Figure 25: pressure at v=1.72 m/s - 1600 rpm.

CFD analyzes were performed between 800 rpm and 1600 rpm at a flow rate of 1.72 m/s (see Figure 16, Figure 17, Figure 18, Figure 19, Figure 20, Figure 21, Figure 22, Figure 23, Figure 24, Figure 25). The pressure value increased proportionally up to 1400 rpm. After this value, no change was observed in the pressure value as in the previous analyses. When the flow rate was changed from 1.2 m/s to 1.72 m/s, the changes in the fluid field were directly proportional. For both analysis groups, 1400 rpm was found to be the efficient rotational speed for the system.

5. Experimental Calculation of Magnus Lift Force

The Magnus lift force values produced by the rotating cylinder depending on the fluid velocity and cylinder rotation speed were calculated by the towing experiment (see Figure 26). Two cylinders, whose rotation speed and direction can be controlled, were mounted on the sides of the boat model. While the model boat was moving at a constant speed, the roll angles of the boat were examined depending on the change in the rotational speed of the cylinders.

Figure 26: Model boat prepared for towing experiment.

In the towing experiments, four laps of pulling were performed. In the first two laps, the boat was moved at a speed of 1.2 m/s, in the last two laps the boat was moved at a speed of 1.72 m/s. While the boat was moving at a constant speed, the effect of the rotation speed on the Magnus lift force was investigated by changing the cylinder rotation speeds (see Table 1).

Table 1: Boat speed - cylinders rotational speed at towing experiment

Lap	Boat Speed (m/s)	Rotational Speed (rpm)
1	1,2	800
1	1,2	1000
1	1,2	1200
1	1,2	1400
2	1,2	1600
2	1,2	1800
2	1,2	2000

3	1,72	800
3	1,72	1000
3	1,72	1200
4	1,72	1400
4	1,72	1600
4	1,72	1800

As shown in Table 1, the rotational speeds of the cylinders were changed while the boat was moving at a constant speed. Cylinders rotated at the same speed but in different directions. In this way, the boat inclined with Magnus lift force (see Figure 27). The instant roll angle values of the boat were transferred to the computer with the Phyphox software using the sensors on the android device. In Figure 28, Figure 29, Figure 30, Figure 31 and Figure 33 time dependent graphs of the boat's roll angle with the Magnus lift produced by the cylinders are shown.

Figure 27: Heeling of the boat with Magnus lift force

While the boat was moving at speed of 1,2 m/s in the first lap, the cylinders were rotated at 800 rpm, 1000 rpm, 1200 rpm and 1400 rpm. In the first 17 seconds, the cylinders rotated at 800 rpm, while the boat inclined an average of 5,3 degrees. Between the 20th second and the 28th second, the boat inclined 6,6 degrees while the cylinders speed was 1000 rpm. In the 32nd second, the cylinder rotation speed was increased to 1200 rpm, at this speed, the angle of roll changed little, reaching 6,9 degrees. Between the 70th and 80th seconds of the first lap, the boat inclined 7,1 degrees when the cylinders were rotated at 1400 rpm (see Figure 18).

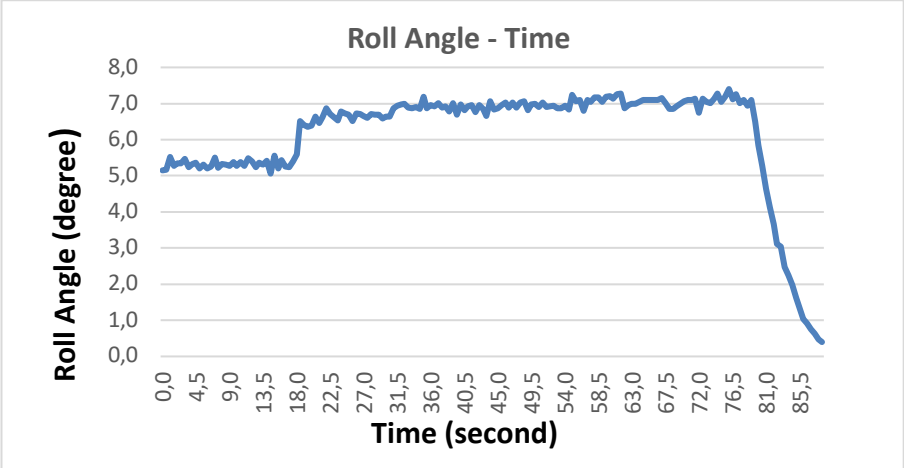

Figure 28: Roll angle – time graph at first lap

The boat was towed again with a speed of 1.2 m/s in the second lap. The changes in the Magnus lift force according to the rotational speed in the constant velocity fluid field were investigated. The cylinders were rotated at 1600 rpm between the 9th and 20th seconds. With the resulting Magnus lift force, the boat inclined 7,2 degrees. In the following lap, cylinder rotation speeds were increased to 1800 rpm, 2000 rpm and 2200 rpm, respectively. No significant change was observed in the inclination angle values of the boat with the increase of the cylinder rotation speed after 1600 rpm (See Figure 19 and Table 2).

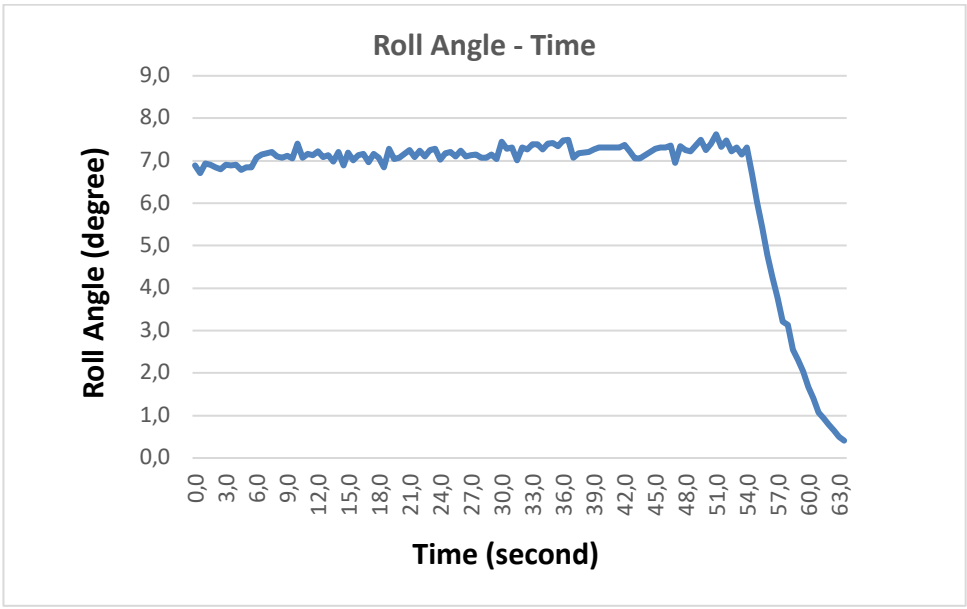

Figure 29: Roll angle – time graph at second lap

Table 2: Effective roll angle values at a flow velocity of 1.2 m/s

Flow velocity (m/s)	Rotational Speed (rpm)	Roll Angle (degree)
1,2	800	5,3
1,2	1000	6,6

1,2	1200	6,9
1,2	1400	7,1
1,2	1600	7,2
1,2	1800	7,2
1,2	2000	7,2
1,2	2400	7,3
1,2	3000	7,3

In order to observe the effect of flow velocity on Magnus lift force, the boat speed was increased to 1,72 m/s in the 3rd and 4th laps. Cylinders were rotated with the same rotational speeds as in the first second laps.

While the boat was moving at a speed of 1,72 m/s in the third lap, cylinders were rotated at 800 rpm, 1000 rpm, 1200 rpm. In Figure 20, the roll angles of the boat due to the Magnus lift force in the third lap are shown. In the third lap, between the 4th and 10th seconds, the boat inclined 8,2 degrees while the cylinders speed was 800 rpm. After the 14th second, inclination angle of the boat reached a value of 10,1 degrees by increasing the rotation speed to 1000 rpm. Boat inclines 10,2 degrees when the cylinder speed reached 1200 rpm.

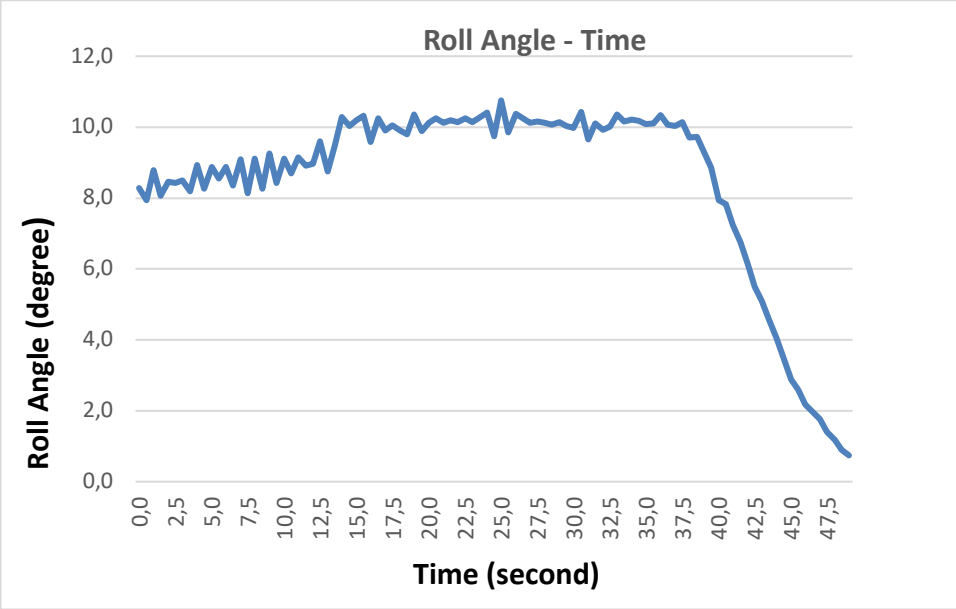

Figure 30: Roll angle - time graph at third lap

In the fourth towing lap, the boat was moved at a speed of 1,72 m/s, while the cylinders were rotated at speeds of 1400 rpm, 1600 rpm, 1800 rpm and 2000 rpm. When the cylinders rotation speed was increased from 1400 rpm to 1600 rpm, boat roll angle increased from 11,1 degrees to 11,9 degrees. The increase in the cylinder speed after 1600 rpm did not cause a significant change in the boat inclination angle. In Figure 21, inclination angle values of the boat are shown depending on the change in the cylinder rotation speed at a fluid speed of 1,72 m/s.

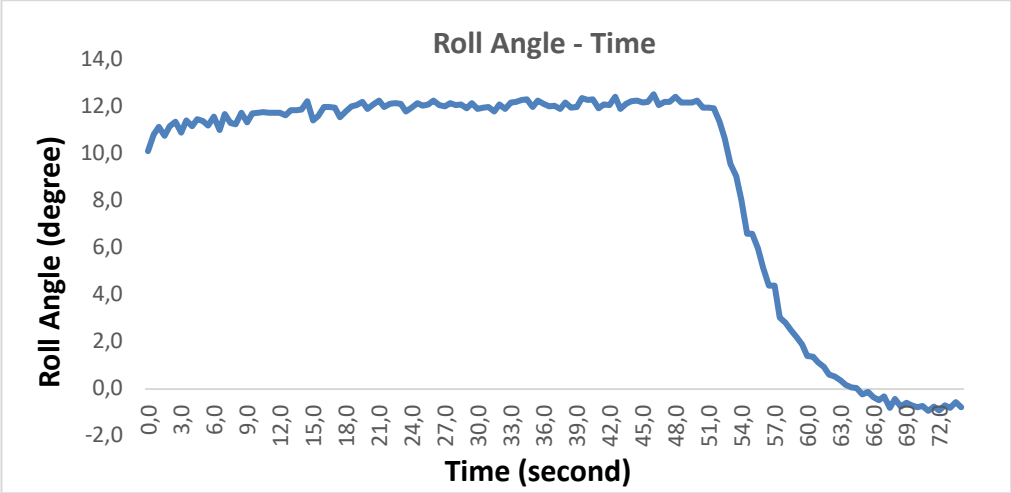

Figure 31: Roll angle - time graph at fourth lap

Table 3: Effective roll angle values at a flow velocity of 1,72 m/s

Flow Velocity (m/s)	Rotational Speed (rpm)	Roll Angle (degree)
1,72	800	8,2
1,72	1000	10,1
1,72	1200	10,2
1,72	1400	11,1
1,72	1600	11,9
1,72	1800	12,1
1,72	2000	12,2

Magnus lift force values produced by the cylinders depending on the rotation speed were calculated with the help of Table 2 and Table 3. In the software environment, different weights were added to the boat at certain distance from the center line. Depending on the different weights added, roll angle values of the boat are shown in Table 4. In Figure 33, the change in roll of boat due to weights placed at a distance of 40 cm from the center line is shown graphically.

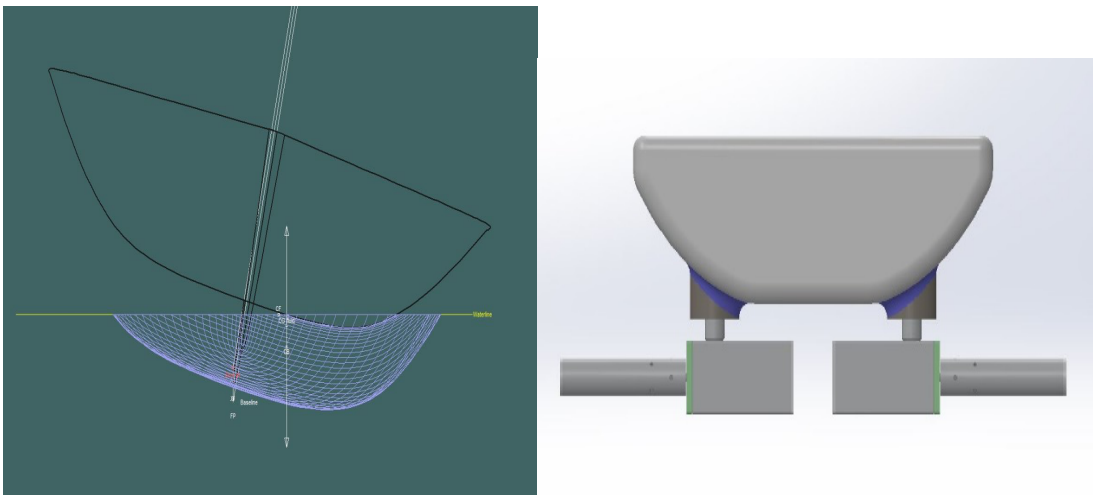

Figure 32: Rolling of the boat with the added weight in the software environment

Table 4: Variation of roll angle values with respect to moment

Mass(kg)	Weight(N)	Moment (N.m)	Angle(degree)
1	9,81	0,4	1,1
2	19,62	0,8	2,2
3	29,43	1,2	3,3
4	39,24	1,6	4,4
5	49,05	2	5,4
6	58,86	2,4	6,4
7	68,67	2,8	7,4
8	78,48	3,2	8,3
9	88,29	3,6	9,3
10	98,1	4	10,3
11	107,91	4,4	11,1
12	117,72	4,8	12
13	127,53	5,2	12,9
14	137,34	5,6	13,8
15	147,15	6	14,5

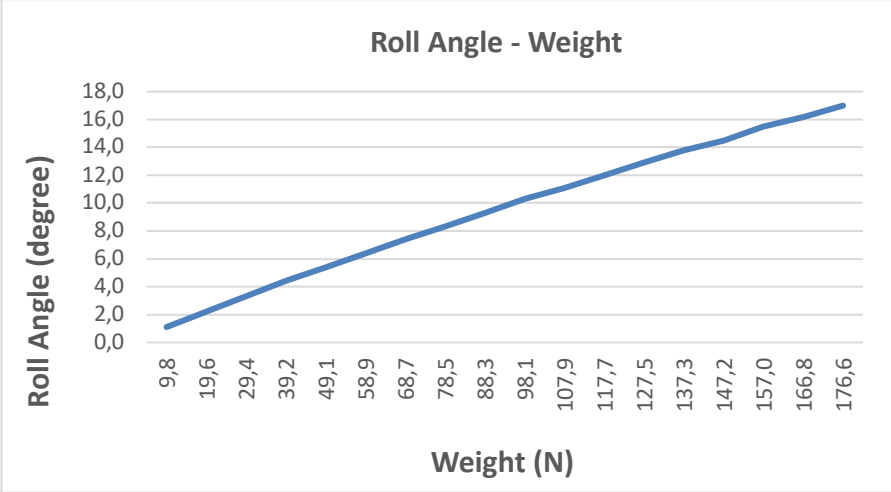

Figure 33: Roll angle - weight graph

The cylinders were mounted to the hull at a distance of 20 cm from the centerline. The work done by the two cylinders together is equivalent to the work done by the weight placed at distance of 40 cm from the centerline (see Figure 23). Magnus lift force values produced by a cylinder with a diameter of 50 mm and a length of 250 mm at different rotational speeds are shown in Table 5.

Table 5: Figure 24: Magnus lift force values depending on parameters

Flow Velocity (m/s)	Rotational Speed (rpm)	Lift Force (N)
1,2	800	24
1,2	1000	30
1,2	1200	32
1,2	1400	34
1,2	1600	35

1,2	1800	35
1,2	2000	35
1,2	2400	35
1,2	3000	35
1,72	800	39
1,72	1200	49
1,72	1400	54
1,72	1600	58
1,72	1800	59
1,72	2000	60

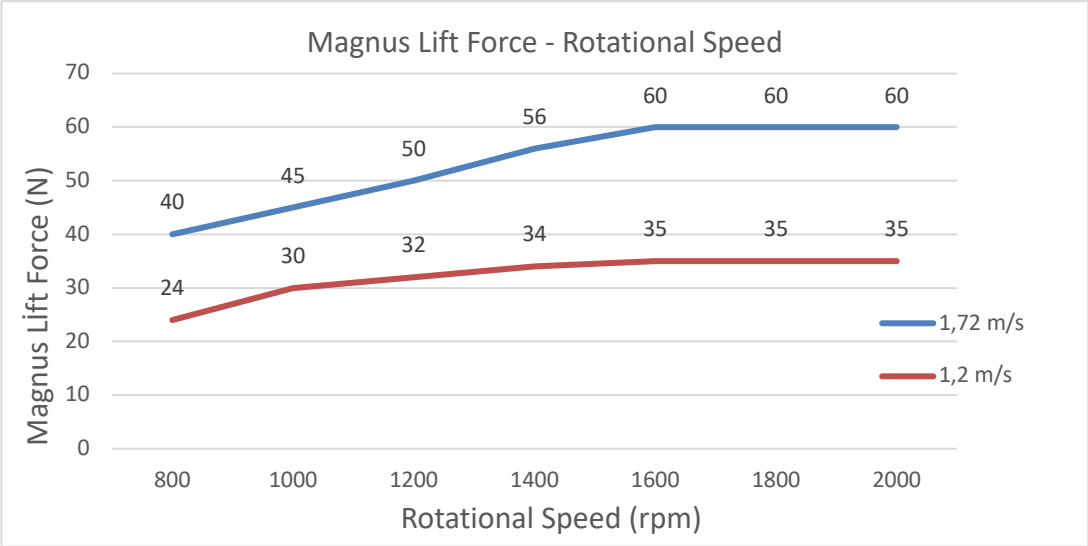

Figure 34: Magnus lift forces graph at 1,2 m/s and 1,72 m/s fluid velocities.

A similar form of change was observed in the Magnus lift force depending on the rotational speed at two different fluid speeds (see Figure 34). Magnus lift force increased proportionally when the rotation speed was increased from 800 rpm to 1400 rpm at a flow rate of 1,2 m/s. Increase in the rotation speed after 1400 rpm did not cause a significant change in the Magnus lift force. A similar situation was observed at a flow rate of 1,72 m/s. But at 1,72 m/s the lift force stabilized after about 1600 rpm. With the experiment, it was concluded that there is a maximum value of Magnus lift force that a fixed length cylinder can produce at certain fluid velocity. After this limit value, the increase in the rotation speed of the cylinder does not cause a change in the Magnus lift force.

6. Conclusions & Recommendations

Analyses were made in Fluent software with the mesh infrastructure prepared for numerical analysis. For 1.2 m/s and 1.72 m/s speeds, the Magnus lifting force increased proportionally with the increase of the rotation speed up to a certain rotation speed. After 1400 rpm, the regime of the flow around the cylinder changed. Frictional effects began to take effect within the flow field. For this reason, numerical analysis gave accurate results only up to 1400 rpm.

The results obtained from the numerical analysis and the results obtained from the experimental study were compared (see Figure 35 and Figure 36). In the experimental study, as in the numerical analysis, a direct proportional increase in the lifting force was observed at a speed of 1400 rpm. After this value, the increase in the cylinder rotation speed did not cause a change in the lifting force. The lift force values obtained from the numerical analysis were greater than the lift forces values observed in the experimental study. This situation was caused by the inability to express the viscous effects sufficiently in numerical analysis. The fluid analysis equations around a rotating cylinder are prepared according to the non-viscous fluid field. Friction effects are included in the analysis with some coefficients. For this reason, the lift force values obtained from the numerical analysis were found to be greater than the values obtained from the experiment.

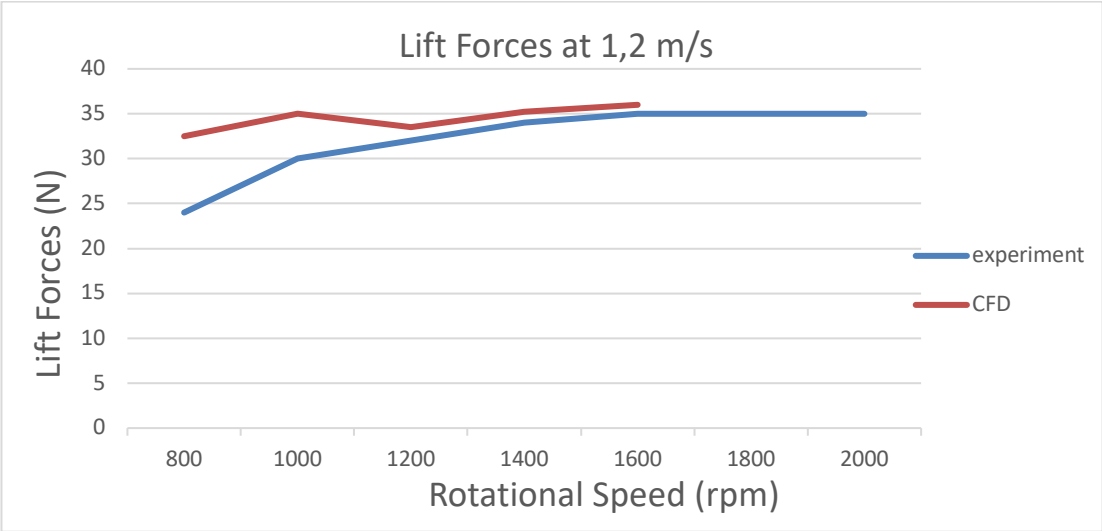

Figure 35: Lift forces at 1.2 m/s

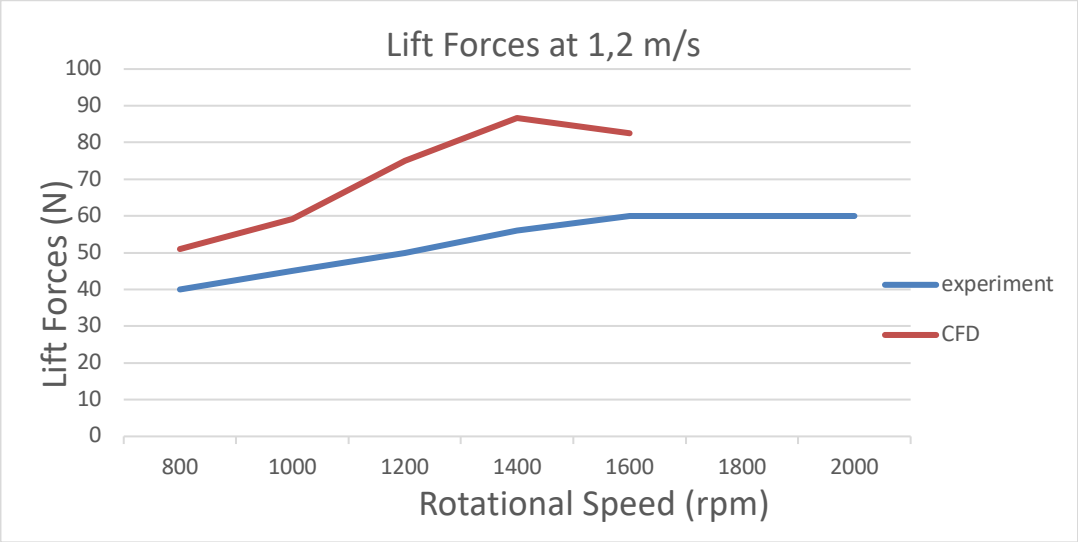

Figure 36: Lift forces at 1,72 m/s

The difference between the values obtained from the numerical calculations and the values obtained from the experimental study increased with the increase of the flow rate. As the fluid velocity increases, the effect of viscous effects in the calculations increases. The ideal cylinder speed for the roll reduction system is in the range of 1200 – 1400 rpm. The Magnus lift force produced at the specified revolution speeds will be sufficient to straighten the model boat. When the model boat is inclined in the range of 5-6 degrees, it will be easily brought to the balance position by the roll reduction system. The system will operate efficiently when the control mechanism of the system changes the direction of rotation of the cylinders at the same time as the roll period of the boat.

Numerical calculations and, most importantly, experiments carried out within the scope of the article showed that the rotating cylinder in the fluid field can produce a force that will bring the boat to the equilibrium position. In addition, the work done is at a very basic level for the design of the roll stabilizing system.

For an efficient roll reduction system design, numerical calculations and experiments should be performed in which the flow around the cylinder is examined according to the variation of different parameters. The parameters to be examined for more efficient system design are listed below.

Experiments were performed using fixed-length cylinders. Changes in Magnus lift force with increasing cylinder length were not investigated. With a telescopic cylinder design, the effect of cylinder length on Magnus lifting force should be examined. As the cylinder length increases, the lift force will increase according to the Kutta-Joukowsky lift theory. However, after a certain point, the change in length will not cause a change in lift force due to viscous effects. Experiments on the appropriate cylinder length should be carried out.

- The effect of cylinder surfaces with different characteristics on the lift force should be examined. Resins that will increase the friction coefficient of the surface can be applied on the roller. With the increase in friction, a later vortex will be observed on the surface. In this way, the cylinder can create lift force at higher rotational speeds.
- The effect on the lifting force by creating roughness on the surface of the cylinder should be examined. The surface of the cylinders used in the experiment was smooth, so the fluid velocity increased with the rotation of the cylinder. Small roughnesses to be formed on the cylinder will

disrupt the flow lines and delay the formation of vortices. The effect of the surface geometry on the buoyancy force should be examined by conducting experiments with the cylinder, which has roughness on its surface according to different parameters.

- Circular cylinders with constant cross-sectional area were used in the experiment. The effect of a rotating body with variable cross-section on the buoyancy should be examined. A larger cross section can be used in the part of the rotor that is closer to the boat hull. The section can be terminated by continuing to decrease the section area towards the end of the cylinder. Thus, the rotor geometry will create less drag force when the system is not active.
- There are studies in the literature showing that by adding a plate to the end of cylinders, higher lifting force is obtained at the same rotational speed. Such a rotor design will create higher drag while the system is inactive. An umbrella-like arrangement can be made at the end of the cylinders to take advantage of the end-plate effect efficiently. If the mechanism at the cylinder end is opened when the system is active, higher lift force value can be achieved. In case the system is not operated, the mechanism closes and the unwanted drag force value decreases.
- The effects of viscous force components in numerical analysis should be examined in more detail. CFD study is based on Kutta – Joukowsky lifting theory. With this theory, calculations are made by ignoring the effects of friction force. CFD studies should be carried out by integrating viscous effects into numerical analysis in order to reduce experimental costs and increase the reliability of calculations in future studies. Thanks to the studies to be carried out in this way, less experiments will be done and more design parameters will be examined.

References

[1] Perez, T., Blanke, M., 2012. Ship roll damping control. Annu. Rev. Control 36, 129–147.

[2] L. H. Liang, M. X. Sun, S. T. Zhang, et al, "Control system design of anti-rolling tank swing bench using BP neural network PID based on LabVIEW," *International Journal of Smart Home*, vol. 9, no. 6, pp. 1-10, 2015.

[3] S.T. Zhang, L. H. Liang and J. F. Wang, "Analysis of real time stabilization effect and parameter optimization of fin stabilizer," *IEEE Int. Conf. Mechatronics Autom.*, *China*, pp. 1103-1108, August 2012.

[4] F. Wang, H. Z. Jin, Z. G. Qi, "Modeling for active fin stabilizers at zero speed," *Ocean Engineering*, vol. 36, pp. 1425-1437, August 2009

[5] Liang, L., Zhao, P., Zhang, S., 2016. Research on hydrodynamic characteristics of magnus rotor wing at medium/low speed. In: Proceedings of IEEE International Conference on Mechatronics and Automation, pp. 539–544.

[6] Liang, L., Zhang, S., He, C., 2012. Predictive control and stabilizing effect analysis of controlled passive tank. In: Proceedings of IEEE International Conference on Mechatronics and Automation, pp. 2547–2552.

[7] Lewis, E., 1989. Principles of Naval Architecture. vol. 3. 2nd ed., SNAME, New Jersey.

[8] Perez, T., 2005. Ship Motion Control: Course Keeping and Roll Stabilisation using Rudder and Fins. Springer-Verlag, London.

[9] Schlichting, H. (1968) Boundary-Layer Theory. Mc Graw-Hill, New York, 364.

[10] Batchelor, G. K. (1967) An Introduction to Fluid Dynamics. Cambridge University Press, Cambridge, UK, plate 1.

[11] Tritton, D.J. (1988) Physical Fluid Dynamics. Oxford Science Publications, New York, 159-161.

[12] Kenyon, K.E. (2013) Flow past a Cylinder. *Journal of Scientific Theory and Methods*, **2013**, 211-222.

[13] Magnus, H., 1852. On the deviation of projectiles; and on a remarkable phenomenon of rotating bodies. Technical Report. Memoirs of the Royal Academy. Berlin.

[14] Prandtl, L., 1926. Application of the Magnus effect to the wind propulsion of ships.

[15] Seifert, J., 2012. A review of the magnus effect in aeronautics. Process Aerosp. Sci. 55, 17–45

[16] Fleming, P., Probert, S., 1984. The evolution of wind-turbines: an historical review. Appl. Energy 18, 163–177.

[17] André, W., Anja, N., 2011. The utilization of the magnus effect for hot water rockets. In: Proceedings of the 20th ESA Symposium on European Rocket and Balloon Programmes and Related Research.

[18] Borg, J., 1980. Magnus effect steering. Mar. Eng. 85, 57–60.

[19] L. Liang, P. Zhao, S. Zhang, J. Yuan, Y. Wen, 2017 "Simulation and analysis of Magnus rotating roll stabilizer at low speed" *Ocean Engineering*, vol. 142, pp. 491-500.

[20] Mittal, S., Kumar, B., 2003. Flow past a rotating cylinder. J. Fluid Mech. 476 (476), 303–334. https://doi.org/10.1017/S0022112002002938.

[21] Mittal, S., 2004. Three-dimensional instabilities in flow past a rotating cylinder. J. Appl. Mech. 71 (1), 89–95. https://doi.org/10.1115/1.1631032.

[22] Dol, S.S., Kopp, G.A., Martinuzzi, R.J., 2008. The suppression of periodic vortex shedding from a rotating circular cylinder. J. Wind Eng. Ind. Aerod. 96 (6–7), 1164–1184. https://doi.org/10.1016/j.jweia.2007.06.038.

[23] Aljure, D.E., Rodríguez, I., Lehmkuhl, O., P´erez-Segarra, C.D., Oliva, A., 2015. Influence of rotation on the flow over a cylinder at Re=5000. Int. J. Heat Fluid Flow. 55, 76–90. https://doi.org/10.1016/j.ijheatfluidflow.2015.07.015.

[24] Karabelas, S.J., Koumroglou, B.C., Argyropoulos, C.D., Markatos, N.C., 2012. High Reynolds number turbulent flow past a rotating cylinder. Appl. Math. Model. 36 (1), 379–398. https://doi.org/10.1016/j.apm.2011.07.032.

[25] Dasgupta, A., Gopalan, H., Chandar, D., 2020. Investigation of flow past rotating cylinder using transitional RANS models for different mesh motion methodologies. AIAA Scitech 2020 Forum. https://doi.org/10.2514/6.2020-1587.

[26] Chen, W., Rheem, C., Zheng, Y., Incecik, A., Lin, Y., Li, Z., 2020. Discrete-vortex analysis of high Reynolds number flow past a rotating cylinder Discrete-vortex analysis of high Reynolds number flow past a rotating cylinder. AIP Adv. 10 (5) https://doi.org/ 10.1063/5.0004851.

[27] Sosa, L.R.P., 2014. The Influence of Reynolds Number, Surface Roughness, and Harmonic Oscillations on a Magnus Effect Rotor. Delft University of Technology.

[28] Sosa, L.R.P., Ooms, J., 2016. A comfort analysis of an 86 m yacht fitted with fin stabilizers vs. Magnus-effect rotors. 24th International HISWA Symposium on Yacht Design and Yacht Construction, pp. 1–13. Amsterdam.

[29] Liang, L., Zhao, P., Zhang, S., 2016. Research on hydrodynamic characteristics of Magnus rotor wing at medium/low speed. In: IEEE International Conference on Mechatronics and Automation, IEEE ICMA 2016, pp. 2413–2418. https://doi.org/10.1109/ ICMA.2016.7558944.

[30] Tu, J., Yeoh, G.H., & Liu, C. (2018). Computational fluid Dynamics: a practical approach. Butterworth – Heinemann.